Nano Research
2019, 12(2): 375–380

ISSN 1998-0124 CN 11-5974/O4
https://doi.org/10.1007/s12274-018-2226-2

Research Article

Nickel cobalt phosphide with three-dimensional nanostructure as a highly efficient electrocatalyst for hydrogen evolution reaction in both acidic and alkaline electrolytes

Bo Ma[1], Zhengchun Yang[2], Yantao Chen[1] (✉), and Zhihao Yuan[1] (✉)

[1] *Tianjin Key Laboratory for Photoelectric Materials and Devices, School of Materials Science and Engineering, Tianjin University of Technology, Tianjin 300384, China*

[2] *School of Electrical and Electronic Engineering, Tianjin Key Laboratory of Film Electronic & Communication Devices, Tianjin University of Technology, Tianjin 300384, China*

Received: 20 August 2018 / **Revised:** 10 October 2018 / **Accepted:** 13 October 2018

ABSTRACT

Transition metal phosphides (TMPs) are promising candidates for noble metal free electrocatalysts in water splitting applications. In this work, we present the facile synthesis of nickel cobalt phosphide electrocatalyst with three-dimensional nanostructure (3D-NiCoP) on the nickel foam, via hydrothermal reaction and phosphorization. The as-prepared electrocatalyst exhibits an excellent activity for hydrogen evolution reaction (HER) in both acidic and alkaline electrolytes, with small overpotentials to drive 10 mA/cm^2 (80 mV for 0.5 M H_2SO_4, 105 mV for 1 M KOH), small Tafel slopes (37 mV/dec for 0.5 M H_2SO_4, 79 mV/dec for 1 M KOH), and satisfying durability in long-term electrolysis. 3D-NiCoP also shows a superior HER activity compared to single metal phosphide, such as cobalt phosphide and nickel phosphide. The outstanding performance for HER suggests the great potential of 3D-NiCoP as a highly efficient electrocatalyst for water splitting technology.

KEYWORDS

nickel cobalt phosphide, water splitting, hydrogen evolution reaction, electrocatalyst

1 Introduction

The utilization of clean energy is drawing a lot of attention in recent years, considering the environmental and economic benefits [1]. However, solar power and wind power, as the most important sources of clean energy, cannot offer continuous supply of electricity and are inappropriate for being directly incorporated into the electrical grid [2]. One option is to convert the electricity generated by clean energy into hydrogen fuel through water splitting. The electrocatalyst is critical in hydrogen evolution reaction (HER), since it can greatly reduce the energy consumption during water splitting and thus achieve better energy efficiency. Up to date, noble metal-based materials, such as platinum (Pt), are the most prominent electrocatalysts for HER [3–5], while the scarcity and high-cost are the major drawbacks for the practical applications. Therefore, developing non-noble metal electrocatalysts with activity comparable to noble metal-based materials, becomes a very important topic of hydrogen economy [6–8]. There have been quite a lot of efforts devoted on utilizing inexpensive and earth abundant materials as efficient electrocatalysts for HER. Transition metal dichalcogenides [9–13], selenides [14–17], carbides [18–21], nitrides [22–24] and phosphides [25–32], are attracting considerable attention for their outstanding HER activity, featuring both low overpotential and facile HER kinetics.

In recent years, transition metal phosphides (TMPs), which are well known as hydrogenation catalysts, are also studied as electrocatalysts for HER. Several members of TMPs are especially important, such as molybdenum phosphide [33], tungsten phosphide [26, 34–36], iron phosphide [37–41], nickel phosphide [42–47] and cobalt phosphide [48–56], considering their low cost and outstanding electrocatalytic activity towards HER. Mu et al. successfully developed flexible MoP nanosheet array electrodes via hydrothermal reaction and phosphidation, which showed a superior electrocatalytic activity for HER in a wide pH range [33]. Sung et al. reported the fabrication of carbon-shell-coated FeP nanoparticles, with excellent HER activity in acidic electrolyte [41]. Wang et al. synthesized sponge-like nickel phosphide-carbon nanotube hybrid electrodes, featuring efficient hydrogen evolution over a wide pH range [42]. Furthermore, the electrocatalytic performance of TMP can be enhanced by doping with other transition metals [31, 57]. For example, Gu et al. reported the theoretical calculation and experimental fabrication of $Fe_xCo_yNi_2P$ as a highly efficient HER electrocatalyst in acidic electrolyte, and the optimal HER performance was achieved when Fe, Co, and Ni had the same atomic ratio ($x/y/z = 1$) [57].

Although TMPs have drawn a lot of attention for their excellent activity on HER, few of them exhibited comparable performance to the state-of-the-art Pt/C catalyst in both acidic and alkaline electrolytes. Herein, we reported the fabrication of nickel cobalt phosphide with three-dimensional nanostructure (3D-NiCoP) as a highly efficient electrocatalyst for HER in both acidic and alkaline electrolytes. The overpotentials to drive the current density of 10 mA/cm^2 are 80 mV for 0.5 M H_2SO_4 and 105 mV for 1 M KOH. The Tafel slopes are measured as 37 mV/dec for 0.5 M H_2SO_4 and 79 mV/dec for 1 M KOH, respectively. We also found that 3D-NiCoP can improve the HER performance compared to the single metal phosphide. Moreover, the as-prepared 3D-NiCoP showed excellent durability in both acidic and alkaline electrolytes, with negligible current decay for more

Address correspondence to Yantao Chen, chenyantao@tjut.edu.cn; Zhihao Yuan, zhyuan@tjut.edu.cn

than 16 hours. This study provides a new route for fabricating TMP-based electrocatalyst towards HER, which could pave the way for the design and development of noble metal-free electrocatalyst.

2 Experimental

2.1 Materials

$Ni(Ac)_2{\cdot}4H_2O$, $Co(Ac)_2{\cdot}4H_2O$, 1,3-propanediol, isopropanol and $NaH_2PO_2{\cdot}H_2O$ were purchased from Aladdin Ltd. (Shanghai, China). Nafion solution (5 wt.%) was purchased from Sigma-Aldrich. All chemicals were used as received without any further purification.

2.2 Preparation of 3D-NiCoP and control groups

Synthesis of 3D-NiCoP on the Ni foam (NF). NiCo hydroxides (NiCo-OH) were hydrothermally synthesized on NF, which was pre-cleaned by acetone and 2 M HCl, followed by washing with water and ethanol. In a typical synthesis, 0.7 mmol of $Ni(Ac)_2{\cdot}4H_2O$ and 1.4 mmol of $Co(Ac)_2{\cdot}4H_2O$ were dissolved into 2.4 mL of 1,3-propanediol completely. Then, 37.6 mL of isopropanol was added into the above solution to form a homogeneous solution. Thereafter, the resulting mixture was transferred into a 50 mL Teflon-lined stainless-steel autoclave with three pieces of 1 cm × 2 cm NF (1.6 mm thickness) leaning against the wall, and heated at 160 °C in an oven for 12 h. After cooling down to room temperature naturally, the substrate was taken out and rinsed with ethanol and water. After dried under a flow of nitrogen gas, the NiCo-OH were then thermally phosphorized to give 3D-NiCoP. Briefly, the NF covered with precursor material and 1 g $NaH_2PO_2{\cdot}H_2O$ were placed in two separate quartz boats, with $NaH_2PO_2{\cdot}H_2O$ at the upstream side of a tube furnace and heated at 300 °C for 2 h under an Ar atmosphere with a heating rate of 5 °C/min. As control experiments, the samples fabricated with half and quarter concentrations of $Ni(Ac)_2{\cdot}4H_2O$ and $Co(Ac)_2{\cdot}4H_2O$ (0.35 and 0.7, 0.175 and 0.35 mmol) were synthesized with other conditions unchanged, which were denoted as NiCoP/2 and NiCoP/4, respectively.

Synthesis of NiP_x and CoP_x on the NF. The synthetic method was the same as 3D-NiCoP, except single metal acetate, i.e., 2.1 mmol of $Ni(Ac)_2{\cdot}4H_2O$ or $Co(Ac)_2{\cdot}4H_2O$, was used for preparing the Ni or Co hydroxide precursor.

2.3 Materials characterization

The scanning electron microscopy (SEM) was conducted on a FEI Quanta FEG. The transmission electron microscopy (TEM) was performed on a JEOL JEM-2800. The X-ray diffraction (XRD) patterns were obtained on a Rigaku DMAX-2500 with Cu Kα radiation. The X-ray photoelectron spectroscopy (XPS) was conducted on a ThermoFisher Scientific Escalab 250Xi.

2.4 Electrochemical characterization

The electrochemical measurements for HER were carried out with a CHI 760E electrochemical workstation (Shanghai Chenhua Instrument Co., China) by using a three-electrode setup. The as-prepared electrodes (1 cm × 1 cm), a reversible hydrogen electrode (RHE, for 0.5 M H_2SO_4) or Hg/HgO (for 1 M KOH), and a platinum slice were used as the working electrode, reference electrode and counter electrode, respectively. 1 mg 20% Pt/C powder, 50 μL 5% Nafion solution, 475 μL ethanol and 475 μL deionized (DI) water were mixed with the assistance of ultrasonication to form a homogeneous ink. Then, 200 μL of the ink was dropcast onto one piece of NF (1 cm × 1 cm) to fabricate the Pt/C electrode for comparison of electrocatalytic activity. The polarization curves were recorded with a scan rate of 5 mV/s in Ar-saturated electrolytes (0.5 M H_2SO_4 and 1 M KOH), and the data were iR-corrected for ohmic losses. The measured potentials (vs. Hg/HgO) in 1 M KOH were converted into RHE scale by $E_{RHE} = E_{Hg/HgO} + 0.925$ V. The details of calibrating Hg/HgO reference electrode into RHE are shown in Fig. S1 in the Electronic Supplementary Material (ESM). Electrochemical impedance spectroscopy (EIS) was conducted from 100 kHz to 0.01 Hz with an amplitude of 5 mV.

3 Results and discussion

The schematic illustration of preparing 3D-NiCoP is displayed in Fig. 1(a). The 3D-NiCoP electrocatalysts are fabricated by the growth of NiCo-OH on the NF via hydrothermal reaction first, followed by phosphorization (see the Experimental Section).

The XRD pattern of NiP_x in Fig. S2(a) in the ESM displays the peaks corresponding to the Ni-P compound, in which Ni_2P (PDF No. 65-3544) is the major component. According to the XRD pattern of CoP_x in Fig. S2(b) in the ESM, there are peaks corresponding to CoP (PDF No. 29-0497), and the peaks corresponding to Ni-P compound can also be observed, which can be attributed to the surface phosphorization of NF. The XRD patterns (Fig. 1(b)) clearly suggest that the NiCo–OH precursor was converted into hexagonal NiCoP (space group $P\bar{6}2m$, a = 5.834 Å) after phosphorization. The peaks of 3D-NiCoP at 41.0° and 47.6° can be ascribed to the (111) and (210) planes of hexagonal NiCoP (PDF No. 71-2336) [58]. The asterisk-marked peaks can be assigned to the NF, and the other small peaks can be attributed to the different chemical constitutions of Ni phosphide species [59]. The XRD patterns of NiCoP/2 and NiCoP/4 are very similar to 3D-NiCoP, as shown in Figs. S2(c) and S2(d) in the ESM.

The SEM images show that the surface of bare NF is relatively

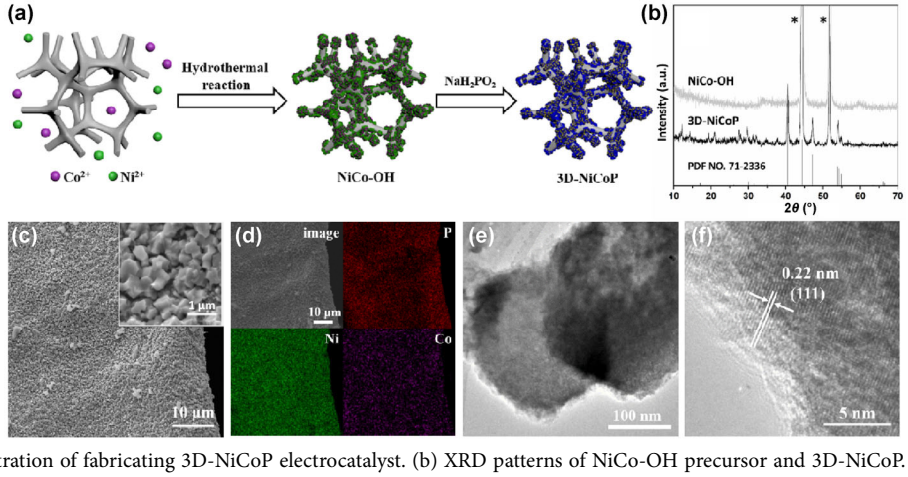

Figure 1 (a) Schematic illustration of fabricating 3D-NiCoP electrocatalyst. (b) XRD patterns of NiCo-OH precursor and 3D-NiCoP. (c) SEM image, (d) elemental mapping of P, Ni and Co, (e) TEM image, (f) HRTEM image of 3D-NiCoP.

smooth (Fig. S3 in the ESM), while the surface of 3D-NiCoP were uniformly covered by densely packed nanocube-like material (Fig. 1(c) and inset). The corresponding energy dispersive X-ray (EDX) elemental mapping (see Fig. 1(d)) reveals that Ni, Co, and P are uniformly distributed over the surface. The EDX spectrum of 3D-NiCoP is displayed in Fig. S4 in the ESM. The TEM image of 3D-NiCoP is presented in Fig. 1(e). A high-resolution transmission electron microscopy (HRTEM) image of 3D-NiCoP (Fig. 1(f)) shows well-resolved lattice fringes with interplanar distances of 0.22 nm, which corresponds to the (111) plane of NiCoP. The selected area electron diffraction (SAED) pattern (Fig. S5 in the ESM) exhibits discrete diffraction rings, which can be indexed to (111), (201), (210) and (211) planes of hexagonal NiCoP. In contrast, the NiCoP/2 and NiCoP/4 have small and sparse nanocube-like structure (Figs. S6(a) and S6(b) in the ESM), while the NiP_x and CoP_x cannot form the nanocube-like structure (Figs. S6(c) and S6(d) in the ESM).

XPS was carried out to determine the chemical composition on the surface of 3D-NiCoP. The XPS survey spectrum is shown in Fig. S7 in the ESM, confirming the presence of Ni, Co, and P. As shown in Fig. 2(a), the peak at 853.5 eV for Ni $2p_{3/2}$ can be ascribed to the presence of partially charged Ni species ($Ni^{\delta+}$, δ is likely close to 0) in Ni-P compound, while the peak located at around 857 eV can be assigned to Ni^{2+} in nickel oxide. For Ni $2p_{1/2}$, the peak corresponding to $Ni^{\delta+}$ in Ni–P compound is located at 869.8 eV and the peak which can be assigned to Ni^{2+} is located at 874.8 eV. The peaks at 863.4 and 880.3 eV are ascribed to the satellites of Ni $2p_{3/2}$ and Ni $2p_{1/2}$, respectively [60, 61]. Similarly, for Co 2p segment (Fig. 2(b)), the Co $2p_{3/2}$ peak at 777.8 eV suggests that there are reduced Co species ($Co^{\delta+}$, δ is likely close to 0) in the Co–P compound, which are also partially charged. In addition, the peaks at 782.2 eV in the Co $2p_{3/2}$ region and 799.2 eV in the Co $2p_{1/2}$ region are assigned to the oxidized Co species ($Co^{2+/3+}$). The remaining two peaks deconvoluted at 787 and 804 eV are satellite peaks [49, 62]. A high resolution spectra of the P 2p region (Fig. 2(c)) presents the peaks at 129.5 and 134.5 eV, which can be assigned to the reduced phosphorus in the form of metal phosphides and the oxidized phosphorous (denoted as P^{5+}) due to the exposure to air [63].

The HER activities of the as-prepared electrocatalysts were initially tested in Ar-saturated 0.5 M H_2SO_4 solution using a three-electrode setup. Figure 3(a) displays the polarization curves of 3D-NiCoP, control groups and commercial Pt/C. The overpotential required to drive the current density of 10 mA/cm^2 (η_{10}) is often used to compare the electrocatalytic activity for HER. 3D-NiCoP exhibits a small η_{10} as low as 80 mV, which is comparable to commercial Pt/C, implying the low energy consumption during the electrocatalytic process. Pt and graphite rod are the most widely used counter electrodes for HER. The polarization curve of one freshly prepared 3D-NiCoP was measured in 0.5 M H_2SO_4 with graphite rod and compared with Pt, as shown in Fig. S8(a) in the ESM. 3D-NiCoP samples, which were measured with different counter electrodes, have almost overlapped polarization curves and equal η_{10} (80 mV), indicating that different counter electrodes have negligible impact on the performance. For other control groups, they show decreased HER activities, with η_{10} determined as 95, 101, 120, 128 and 205 mV for NiCoP/2, NiCoP/4, NiP_x, CoP_x and NF, respectively. To study the HER mechanism of the as-prepared electrocatalysts, the Tafel slopes were obtained by fitting the linear portions of the Tafel plots (Fig. 3(b)) to the Tafel equation ($\eta = b\log|j| + a$, where j is the current density and b is the Tafel slope). The typical HER process involves three steps distinguished by different Tafel slopes, including Volmer (120 mV/dec), Heyrovsky (40 mV/dec) and Tafel (30 mV/dec) reactions [64]. Pt/C exhibits the smallest Tafel slope of 27 mV/dec, indicating the Volmer-Tafel HER mechanism ($H_3O^+ + e^- \rightarrow H_{ads}$, $H_{ads} + H_{ads} \rightarrow H_2$). For the as-prepared electrocatalysts, the Tafel slopes are 37, 57, 63, 66, 78, 119 mV/dec for 3D-NiCoP, NiCoP/2, NiCoP/4, NiP_x, CoP_x and NF, respectively, suggesting the Volmer-Heyrovsky HER mechanism ($H_3O^+ + e^- \rightarrow H_{ads}$, $H_{ads} + H_3O^+ + e^- \rightarrow H_2 + H_2O$). It is noteworthy that 3D-NiCoP has a Tafel slope close to Pt/C, revealing the electron transfer during HER process is facilitated. The exchange current density (j_0) of 3D-NiCoP was 0.094 mA/cm^2, which was obtained by extrapolating the Tafel plot to x-axis (Fig. S9 in the ESM). EIS was conducted at the potential of −80 mV (vs. RHE) to study the HER kinetics of 3D-NiCoP and the other electrocatalysts. The Nyquist plots of the as-prepared electrocatalysts are displayed in Fig. 3(c). The diameter of the semicircle represents the charge transfer resistance (R_{ct}). The values of R_{ct} are obtained by fitting the data to an equivalent circuit (inset of Fig. 3(c)). 3D-NiCoP exhibits the smallest R_{ct} value (3.37 Ω), while the R_{ct} values for NiCoP/2, NiCoP/4, NiP_x, CoP_x and NF are 5.9, 6.9, 13.2, 14.7 and 88 Ω, respectively. The small R_{ct} value of 3D-NiCoP indicates the facile charge transfer, leading to an enhanced HER activity. The series resistance (R_s) values in 0.5 M H_2SO_4 are shown in Table S1 in the ESM. In addition, the durability of electrocatalyst is also a critical factor for the water splitting application. The long-term electrolysis was conducted at a constant potential of −83 mV (vs. RHE) in 0.5 M H_2SO_4 to examine the durability of 3D-NiCoP in the HER process (Fig. 3(d)). The current density fluctuation, as shown in the inset of Fig. 3(d), can be attributed to the bubble formation and release. A 99.5% current retention was observed after 16 hours' continuous operation, suggesting the satisfying long-term durability of 3D-NiCoP. The morphology of 3D-NiCoP after the durability test in 0.5 M H_2SO_4 is very similar to original 3D-NiCoP, as shown in the SEM image in Fig. S10(a) in the ESM.

The HER activity of electrocatalysts in alkaline electrolyte is also very important, considering the water splitting is often carried out in alkaline electrolyte in industry. The as-prepared electrocatalysts were tested again in Ar-saturated 1 M KOH solution with three-electrode setup. Figure 4(a) presents the polarization curves of the electrocatalysts in 1 M KOH. The values of η_{10} for 3D-NiCoP, NiCoP/2, NiCoP/4, NiP_x, CoP_x and NF are determined as 105, 139, 155, 148,

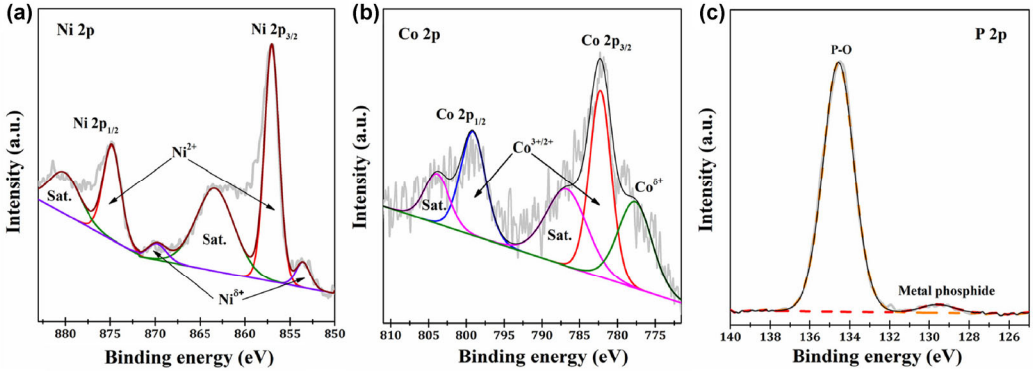

Figure 2 High-resolution XPS spectra of the 3D-NiCoP. (a) Ni 2p, (b) Co 2p, and (c) P 2p.

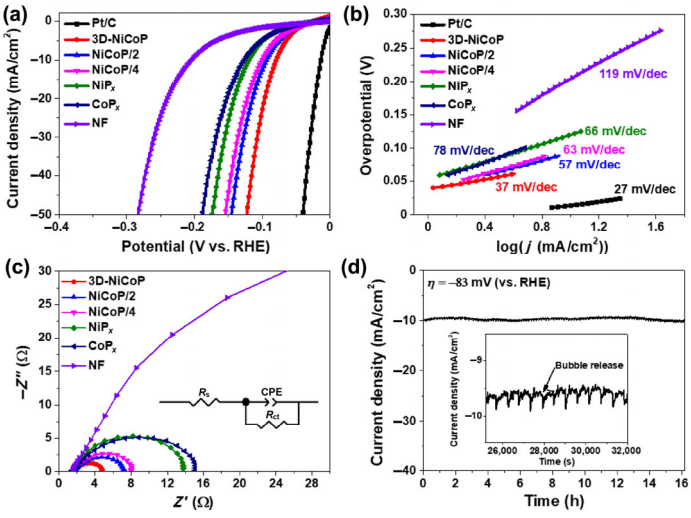

Figure 3 HER activity of the as-prepared electrocatalysts in Ar-saturated 0.5 M H_2SO_4. (a) Polarization curves recorded with a scan rate of 5 mV/s. (b) Tafel plots derived from (a). (c) Nyquist plots with equivalent circuit (inset). The EIS was conducted at −80 mV (vs. RHE). (d) Long-term durability test at −83 mV (vs. RHE).

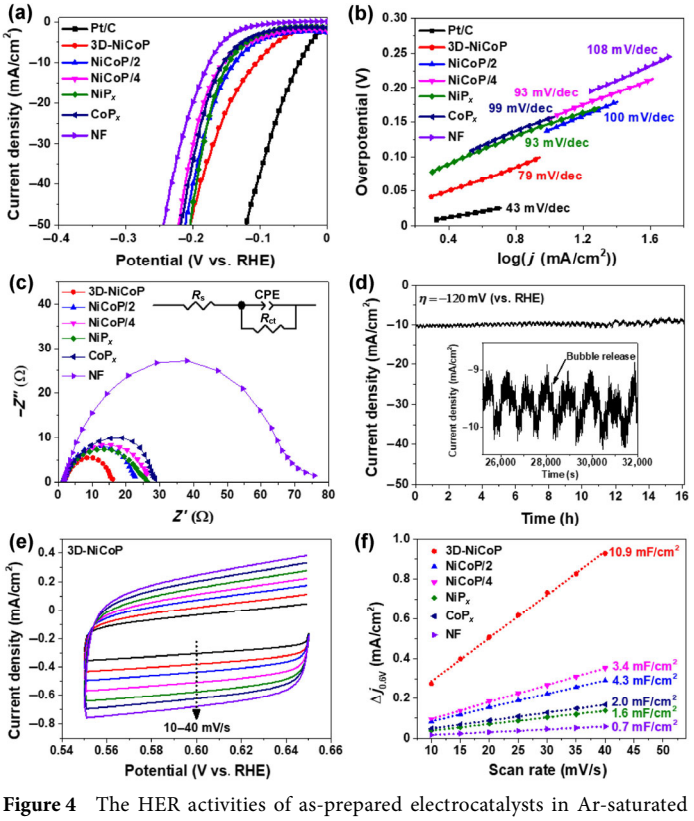

Figure 4 The HER activities of as-prepared electrocatalysts in Ar-saturated 1 M KOH. (a) Polarization curves recorded with a scan rate of 5 mV/s. (b) Tafel plots derived from (a). (c) Nyquist plots with equivalent circuit (inset). The EIS was conducted at −100 mV (vs. RHE). (d) Long-term durability test at −120 mV (vs. RHE). (e) Cyclic voltammetry of 3D-NiCoP by sweeping from 0.55 to 0.65 V (vs. RHE) at different scan rates (10, 15, 20, 25, 30, 35, 40 mV/s). (f) The capacitive currents measured at the potential of 0.6 V (vs. RHE) were plotted against the scan rate for estimation of C_{dl} by linear fitting the corresponding plots.

155 and 165 mV, respectively. The polarization curve of freshly prepared 3D-NiCoP in 1 M KOH with graphite rod as counter electrode is compared with Pt and shown in Fig. S8(b) in the ESM, which suggests almost equal η_{10} (105 mV for Pt and 109 mV for graphite rod) and the negligible impact on performance with different counter electrodes. The sluggish HER kinetics in alkaline electrolytes often impedes the practical application of electrocatalysts. In order to study the HER kinetics, the Tafel plots are presented in Fig. 4(b). Unsurprisingly, commercial Pt/C yields the smallest Tafel slope of 43 mV/dec. 3D-NiCoP exhibits a Tafel slope of 79 mV/dec, suggesting 3D-NiCoP proceeds through the Volmer-Heyrovsky mechanism ($H_2O + e^- \rightarrow H_{ads} + OH^-$, $H_2O + e^- + H_{ads} \rightarrow H_2 + OH^-$) in 1 M KOH. It should be noted that 3D-NiCoP has a smaller Tafel slope than NiCoP/2 (100 mV/dec), NiCoP/4 (93 mV/dec), NiP$_x$ (93 mV/dec), CoP$_x$ (99 mV/dec) and NF (108 mV/dec), revealing the excellent HER kinetics of 3D-NiCoP among the as-prepared electrocatalysts. The Nyquist plots of the electrocatalysts are displayed in Fig. 4(c) to further examine the HER kinetics in 1 M KOH. The R_s values in 1 M KOH are listed in Table S1 in the ESM. 3D-NiCoP still exhibits the smallest R_{ct} value (14.8 Ω), while the R_{ct} values for NiCoP/2, NiCoP/4, NiP$_x$, CoP$_x$ and NF, are determined as 21.4, 25.4, 24.1, 27.7 and 68.9 Ω, respectively. The EIS data indicates 3D-NiCoP is more favorable for rapid electron transfer during HER process, revealing the superior HER activity of 3D-NiCoP compared to other electrocatalysts. The long-term durability of 3D-NiCoP is also very encouraging, with a 95.1% current retention after 16 hours' continuous electrolysis at the potential of −120 mV (vs. RHE), implying the negligible activity decay during HER process. Besides, the SEM image of 3D-NiCoP after the durability test in 1 M KOH is shown in Fig. S10(b) in the ESM, with similar morphology to the original 3D-NiCoP. In order to compare the electrochemical active surface area (ECSA) of the electrocatalysts, double layer capacitances (C_{dl}) were measured by performing cyclic voltammetry from 0.55 to 0.65 V (vs. RHE) and then plotting the current density variation ($\Delta j = j_{anode} - j_{cathode}$) at 0.6 V (vs. RHE) against scan rates, as shown in Figs. 4(e) and 4(f). The cyclic voltammetry curves of NiCoP/2, NiCoP/4, NiP$_x$ and CoP$_x$ are presented in Fig. S11 in the ESM. The values of C_{dl} can be estimated by half of the slope in Fig. 4(f), which are determined as 10.9, 4.3, 3.4, 1.6, 2.0 and 0.7 mF/cm^2 for 3D-NiCoP, NiCoP/2, NiCoP/4, NiP$_x$, CoP$_x$ and NF, respectively. Considering the ECSA is proportional to C_{dl}, 3D-NiCoP has the largest ECSA among the as-prepared electrocatalysts, which is more favorable for electrochemical reactions.

The HER activities of 3D-NiCoP and other recently reported TMP-based electrocatalysts are listed in Tables S2 (acidic electrolyte) and S3 (alkaline electrolyte) in the ESM. 3D-NiCoP exhibits excellent electrocatalytic activities in both acidic and alkaline electrolytes, featuring a low η_{10}, a small Tafel slope and remarkable long-term durability. More importantly, 3D-NiCoP showed an enhanced HER activity compared to NiP$_x$ and CoP$_x$, revealing the advantage of combining different TMPs. The excellent electrocatalytic performance of 3D-NiCoP can be attributed to the following reasons. First, the electrocatalysts are commonly designed as one-dimensional nanowires or two-dimensional nanosheets to efficiently avoid the aggregation, while the surface coverage ratio of the as-synthesized nanomaterials on the substrate (carbon cloth and NF) is decreased accordingly. The three-dimensional nanostructure of 3D-NiCoP can efficiently avoid the aggregation for exposing more active sites, as well as achieving a high surface coverage ratio on NF. Secondly, the density functional theory (DFT) calculations showed that NiCoP can significantly lower the Gibbs free energy of hydrogen adsorption compared to the single metal phosphides, leading to an improved HER performance [58]. Thirdly, water molecules can be strongly adsorbed on the surface of NiCoP [58], with H–OH bonds weakened by the interactions between metal center and O atom as well as dangling P atom and H atom, which facilitates the dissociation of water molecules for rapid HER kinetics in alkaline electrolytes [31].

4 Conclusions

In summary, 3D-NiCoP electrocatalysts were fabricated via hydrothermal reaction and phosphorization. 3D-NiCoP has a densely packed nanocube-like structure, with higher surface coverage ratio

of electrocatalysts on the substrate. As a demonstration, 3D-NiCoP exhibits excellent HER activity in both acidic and alkaline electrolytes, with low overpotentials, small Tafel slopes as well as satisfying long-term durability, which can be attributed to the synergistic effect of multiple factors, including the three-dimensional nanostructure, optimized Gibbs free energy of hydrogen adsorption and enhanced water molecules adsorption. The successful design, fabrication and characterization of 3D-NiCoP as a highly efficient HER electrocatalyst, demonstrate its promising future for scale-up applications of water splitting technology.

Acknowledgements

This work was supported by the National Natural Science Foundation of China (No. 51702234).

Electronic Supplementary Material: Supplementary material (RHE calibration of Hg/HgO reference electrode, XRD patterns of control groups, SEM image of bare Ni foam, EDX spectrum and atomic ratio, SAED pattern of 3D-NiCoP, SEM images of control groups, XPS survey spectrum, polarization curves of 3D-NiCoP with Pt and graphite rod as counter electrode, estimation of exchange current density, SEM images after durability test, cyclic voltammetry curves of control groups, values of R_s and the comparison results of the electrocatalytic activity towards HER between this work and the reported works) is available in the online version of this article at https://doi.org/10.1007/s12274-018-2226-2.

References

[1] Dresselhaus, M. S.; Thomas, I. L. Alternative energy technologies. *Nature* **2001**, *414*, 332–337.

[2] Cook, T. R.; Dogutan, D. K.; Reece, S. Y.; Surendranath, Y.; Teets, T. S.; Nocera, D. G. Solar energy supply and storage for the legacy and nonlegacy worlds. *Chem. Rev.* **2010**, *110*, 6474–6502.

[3] Chao, T. T.; Luo, X.; Chen, W. X.; Jiang, B.; Ge, J. J.; Lin, Y.; Wu, G.; Wang, X. Q.; Hu, Y. M.; Zhuang, Z. B. et al. Atomically dispersed copper–platinum dual sites alloyed with palladium nanorings catalyze the hydrogen evolution reaction. *Angew. Chem.* **2017**, *129*, 16263–16267.

[4] Ge, J. J.; Wei, P.; Wu, G.; Liu, Y. D.; Yuan, T. W.; Li, Z. J.; Qu, Y. T.; Wu, Y.; Li, H.; Zhuang, Z. B. et al. Ultrathin palladium nanomesh for electrocatalysis. *Angew. Chem.* **2018**, *130*, 3493–3496.

[5] Chen, Y. J.; Ji, S. F.; Chen, C.; Peng, Q.; Wang, D. S.; Li, Y. D. Single-atom catalysts: Synthetic strategies and electrochemical applications. *Joule* **2018**, *2*, 1242–1264.

[6] Wu, G.; Chen, W. X.; Zheng, X. S.; He, D. P.; Luo, Y. Q.; Wang, X. Q.; Yang, J.; Wu, Y.; Yan, W. S.; Zhuang, Z. B. et al. Hierarchical Fe-doped NiO_x nanotubes assembled from ultrathin nanosheets containing trivalent nickel for oxygen evolution reaction. *Nano Energy* **2017**, *38*, 167–174.

[7] Wang, X. Q.; Chen, Z.; Zhao, X. Y.; Yao, T.; Chen, W. X.; You, R.; Zhao, C. M.; Wu, G.; Wang, J.; Huang, W. X. et al. Regulation of coordination number over single Co sites: Triggering the efficient electroreduction of CO_2. *Angew. Chem.* **2018**, *130*, 1962–1966.

[8] Wang, J.; Xu, F.; Jin, H. Y.; Chen, Y. Q.; Wang, Y. Non-noble metal-based carbon composites in hydrogen evolution reaction: Fundamentals to applications. *Adv. Mater.* **2017**, *29*, 1605838.

[9] Li, Y. G.; Wang, H. L.; Xie, L. M.; Liang, Y. Y.; Hong, G. S.; Dai, H. J. MoS_2 nanoparticles grown on graphene: An advanced catalyst for the hydrogen evolution reaction. *J. Am. Chem. Soc.* **2011**, *133*, 7296–7299.

[10] Lukowski, M. A.; Daniel, A. S.; Meng, F.; Forticaux, A.; Li, L. S.; Jin, S. Enhanced hydrogen evolution catalysis from chemically exfoliated metallic MoS_2 nanosheets. *J. Am. Chem. Soc.* **2013**, *135*, 10274–10277.

[11] Sun, W. Y.; Li, P.; Liu, X.; Shi, J. J.; Sun, H. M.; Tao, Z. L.; Li, F. J.; Chen, J. Size-controlled MoS_2 nanodots supported on reduced graphene oxide for hydrogen evolution reaction and sodium-ion batteries. *Nano Res.* **2017**, *10*, 2210–2222.

[12] Sun, K. A.; Liu, Y. Q.; Pan, Y.; Zhu, H. Y.; Zhao, J. C.; Zeng, L. Y.; Liu, Z.; Liu, C. G. Targeted bottom-up synthesis of 1T-phase MoS_2 arrays with high electrocatalytic hydrogen evolution activity by simultaneous structure and morphology engineering. *Nano Res.* **2018**, *11*, 4368–4379.

[13] Chen, Y. T.; Ren, R.; Wen, Z. H.; Ci, S. Q.; Chang, J. B.; Mao, S.; Chen, J. H. Superior electrocatalysis for hydrogen evolution with crumpled graphene/tungsten disulfide/tungsten trioxide ternary nanohybrids. *Nano Energy* **2018**, *47*, 66–73.

[14] Kong, D. S.; Wang, H. T.; Lu, Z. Y.; Cui, Y. $CoSe_2$ nanoparticles grown on carbon fiber paper: An efficient and stable electrocatalyst for hydrogen evolution reaction. *J. Am. Chem. Soc.* **2014**, *136*, 4897–4900.

[15] Zhang, J. T.; Chen, Y. L.; Liu, M.; Du, K.; Zhou, Y.; Li, Y. P.; Wang, Z. J.; Zhang, J. 1T@2H-$MoSe_2$ nanosheets directly arrayed on Ti plate: An efficient electrocatalytic electrode for hydrogen evolution reaction. *Nano Res.* **2018**, *11*, 4587–4598.

[16] Wang, F. M.; Li, Y. C.; Shifa, T. A.; Liu, K. L.; Wang, F.; Wang, Z. X.; Xu, P.; Wang, Q. S.; He, J. Selenium-enriched nickel selenide nanosheets as a robust electrocatalyst for hydrogen generation. *Angew. Chem., Int. Ed.* **2016**, *55*, 6919–6924.

[17] Chen, T.; Tan, Y. W. Hierarchical $CoNiSe_2$ nano-architecture as a high-performance electrocatalyst for water splitting. *Nano Res.* **2018**, *11*, 1331–1344.

[18] Wang, J. B.; Chen, W. L.; Wang, T.; Bate, N.; Wang, C. L.; Wang, E. B. A strategy for highly dispersed Mo_2C/MoN hybrid nitrogen-doped graphene via ion-exchange resin synthesis for efficient electrocatalytic hydrogen reduction. *Nano Res.* **2018**, *11*, 4535–4548.

[19] Li, J. S.; Wang, Y.; Liu, C. H.; Li, S. L.; Wang, Y. G.; Dong, L. Z.; Dai, Z. H.; Li, Y. F.; Lan, Y. Q. Coupled molybdenum carbide and reduced graphene oxide electrocatalysts for efficient hydrogen evolution. *Nat. Commun.* **2016**, *7*, 11204.

[20] Hu, X. L.; Tang, Y.; Liu, B. H.; Girault, H. H. A nanoporous molybdenum carbide nanowire as an electrocatalyst for hydrogen evolution reaction. *Energy Environ. Sci.* **2014**, *7*, 387–392.

[21] Shi, Z. P.; Nie, K. Q.; Shao, Z.-J.; Gao, B. X.; Lin, H. L.; Zhang, H. B.; Liu, B. L.; Wang, Y. X.; Zhang, Y. H.; Sun, X. H. et al. Phosphorus-Mo_2C@ carbon nanowires toward efficient electrochemical hydrogen evolution: Composition, structural and electronic regulation. *Energy Environ. Sci.* **2017**, *10*, 1262–1271.

[22] Zhu, Y. P.; Chen, G.; Zhong, Y. J.; Zhou, W.; Shao, Z. P. Rationally designed hierarchically structured tungsten nitride and nitrogen-rich graphene-like carbon nanocomposite as efficient hydrogen evolution electrocatalyst. *Adv. Sci.* **2018**, *5*, 1700603.

[23] Ren, B. W.; Li, D. Q.; Jin, Q. Y.; Cui, H.; Wang, C. X. A self-supported porous WN nanowire array: An efficient 3D electrocatalyst for the hydrogen evolution reaction. *J. Mater. Chem. A* **2017**, *5*, 19072–19078.

[24] Lv, Z.; Tahir, M.; Lang, X. W.; Yuan, G.; Pan, L.; Zhang, X. W.; Zou, J. J. Well-dispersed molybdenum nitrides on a nitrogen-doped carbon matrix for highly efficient hydrogen evolution in alkaline media. *J. Mater. Chem. A* **2017**, *5*, 20932–20937.

[25] Wang, M. Q.; Ye, C.; Xu, M. W.; Bao, S. J. MoP nanoparticles with a P-rich outermost atomic layer embedded in N-doped porous carbon nanofibers: Self-supported electrodes for efficient hydrogen generation. *Nano Res.* **2018**, *11*, 4728–4734.

[26] Xing, Z. C.; Liu, Q.; Asiri, A. M.; Sun, X. P. High-efficiency electrochemical hydrogen evolution catalyzed by tungsten phosphide submicroparticles. *ACS Catal.* **2015**, *5*, 145–149.

[27] Pan, Y.; Chen, Y. J.; Lin, Y.; Cui, P. X.; Sun, K. A.; Liu, Y. Q.; Liu, C. G. Cobalt nickel phosphide nanoparticles decorated carbon nanotubes as advanced hybrid catalysts for hydrogen evolution. *J. Mater. Chem. A* **2016**, *4*, 14675–14686.

[28] Yang, J.; Zhang, F. J.; Wang, X.; He, D. S.; Wu, G.; Yang, Q. H.; Hong, X.; Wu, Y.; Li, Y. D. Porous molybdenum phosphide nano-octahedrons derived from confined phosphorization in UIO-66 for efficient hydrogen evolution. *Angew. Chem., Int. Ed.* **2016**, *55*, 12854–12858.

[29] Wang, X. D.; Xu, Y. F.; Rao, H. S.; Xu, W. J.; Chen, H. Y.; Zhang, W. X.; Kuang, D. B.; Su, C. Y. Novel porous molybdenum tungsten phosphide hybrid nanosheets on carbon cloth for efficient hydrogen evolution. *Energy Environ. Sci.* **2016**, *9*, 1468–1475.

[30] Xu, K.; Cheng, H.; Lv, H. F.; Wang, J. Y.; Liu, L. Q.; Liu, S.; Wu, X. J.; Chu, W. S.; Wu, C. Z.; Xie, Y. Controllable surface reorganization engineering on cobalt phosphide nanowire arrays for efficient alkaline hydrogen evolution reaction. *Adv. Mater.* **2018**, *30*, 1703322.

[31] Zhang, R.; Wang, X. X.; Yu, S. J.; Wen, T.; Zhu, X. W.; Yang, F. X.; Sun, X. N.; Wang, X. K.; Hu, W. P. Ternary $NiCo_2P_x$ nanowires as pH-universal electrocatalysts for highly efficient hydrogen evolution reaction. *Adv. Mater.* **2017**, *29*, 1605502.

[32] Li, Y. J.; Zhang, H. C.; Jiang, M.; Kuang, Y.; Sun, X. M.; Duan, X. Ternary NiCoP nanosheet arrays: An excellent bifunctional catalyst for alkaline overall water splitting. *Nano Res.* **2016**, *9*, 2251–2259.
[33] Pu, Z. H.; Wei, S. Y.; Chen, Z. B.; Mu, S. C. Flexible molybdenum phosphide nanosheet array electrodes for hydrogen evolution reaction in a wide pH range. *Appl. Catal. B: Environ.* **2016**, *196*, 193–198.
[34] Pu, Z. H.; Liu, Q.; Asiri, A. M.; Sun, X. P. Tungsten phosphide nanorod arrays directly grown on carbon cloth: A highly efficient and stable hydrogen evolution cathode at all pH values. *ACS Appl. Mater. Interfaces* **2014**, *6*, 21874–21879.
[35] Pu, Z. H.; Ya, X.; Amiinu, I. S.; Tu, Z. K.; Liu, X. B.; Li, W. Q.; Mu, S. C. Ultrasmall tungsten phosphide nanoparticles embedded in nitrogen-doped carbon as a highly active and stable hydrogen-evolution electrocatalyst. *J. Mater. Chem. A* **2016**, *4*, 15327–15332.
[36] Wu, L.; Pu, Z. H.; Tu, Z. K.; Amiinu, I. S.; Liu, S. J.; Wang, P. Y.; Mu, S. C. Integrated design and construction of WP/W nanorod array electrodes toward efficient hydrogen evolution reaction. *Chem. Eng. J.* **2017**, *327*, 705–712.
[37] Yan, Y.; Shi, X. R.; Miao, M.; He, T.; Dong, Z. H.; Zhan, K.; Yang, J. H.; Zhao, B.; Xia, B. Y. Bio-inspired design of hierarchical FeP nanostructure arrays for the hydrogen evolution reaction. *Nano Res.* **2018**, *11*, 3537–3547.
[38] Zhu, X. H.; Liu, M. J.; Liu, Y.; Chen, R. W.; Nie, Z.; Li, J. H.; Yao, S. Z. Carbon-coated hollow mesoporous FeP microcubes: An efficient and stable electrocatalyst for hydrogen evolution. *J. Mater. Chem. A* **2016**, *4*, 8974–8977.
[39] Tian, L. H.; Yan, X. D.; Chen, X. B. Electrochemical activity of iron phosphide nanoparticles in hydrogen evolution reaction. *ACS Catal.* **2016**, *6*, 5441–5448.
[40] Li, D. Q.; Liao, Q. Y.; Ren, B. W.; Jin, Q. Y.; Cui, H.; Wang, C. X. A 3D-composite structure of FeP nanorods supported by vertically aligned graphene for the high-performance hydrogen evolution reaction. *J. Mater. Chem. A* **2017**, *5*, 11301–11308.
[41] Chung, D. Y.; Jun, S. W.; Yoon, G.; Kim, H.; Yoo, J. M.; Lee, K. S.; Kim, T.; Shin, H.; Sinha, A. K.; Kwon, S. G. et al. Large-scale synthesis of carbon-shell-coated FeP nanoparticles for robust hydrogen evolution reaction electrocatalyst. *J. Am. Chem. Soc.* **2017**, *139*, 6669–6674.
[42] Wang, S. Y.; Zhang, L.; Li, X.; Li, C. L.; Zhang, R. J.; Zhang, Y. J.; Zhu, H. W. Sponge-like nickel phosphide–carbon nanotube hybrid electrodes for efficient hydrogen evolution over a wide pH range. *Nano Res.* **2017**, *10*, 415–425.
[43] Wang, X. G.; Kolen'ko, Y. V.; Bao, X. Q.; Kovnir, K.; Liu, L. F. One-step synthesis of self-supported nickel phosphide nanosheet array cathodes for efficient electrocatalytic hydrogen generation. *Angew. Chem., Int. Ed.* **2015**, *54*, 8188–8192.
[44] Wang, X. G.; Li, W.; Xiong, D. H.; Petrovykh, D. Y.; Liu, L. F. Bifunctional nickel phosphide nanocatalysts supported on carbon fiber paper for highly efficient and stable overall water splitting. *Adv. Funct. Mater.* **2016**, *26*, 4067–4077.
[45] Han, A. L.; Jin, S.; Chen, H. L.; Ji, H. X.; Sun, Z. J.; Du, P. W. A robust hydrogen evolution catalyst based on crystalline nickel phosphide nanoflakes on three-dimensional graphene/nickel foam: High performance for electrocatalytic hydrogen production from pH 0–14. *J. Mater. Chem. A* **2015**, *3*, 1941–1946.
[46] Pan, Y.; Yang, N.; Chen, Y. J.; Lin, Y.; Li, Y. P.; Liu, Y. Q.; Liu, C. G. Nickel phosphide nanoparticles-nitrogen-doped graphene hybrid as an efficient catalyst for enhanced hydrogen evolution activity. *J. Power Sources* **2015**, *297*, 45–52.
[47] Cao, X. Y.; Jia, D. D.; Li, D.; Cui, L.; Liu, J. Q. One-step co-electrodeposition of hierarchical radial Ni_xP nanospheres on Ni foam as highly active flexible electrodes for hydrogen evolution reaction and supercapacitor. *Chem. Eng. J.* **2018**, *348*, 310–318.
[48] Lu, H. Y.; Fan, W.; Huang, Y. P.; Liu, T. X. Lotus root-like porous carbon nanofiber anchored with CoP nanoparticles as all-pH hydrogen evolution electrocatalysts. *Nano Res.* **2018**, *11*, 1274–1284.
[49] Huang, Z. P.; Chen, Z. Z.; Chen, Z. B.; Lv, C. C.; Humphrey, M. G.; Zhang, C. Cobalt phosphide nanorods as an efficient electrocatalyst for the hydrogen evolution reaction. *Nano Energy* **2014**, *9*, 373–382.
[50] Huang, J. W.; Li, Y. R.; Xia, Y. F.; Zhu, J. T.; Yi, Q. H.; Wang, H.; Xiong, J.; Sun, Y. H.; Zou, G. F. Flexible cobalt phosphide network electrocatalyst for hydrogen evolution at all pH values. *Nano Res.* **2017**, *10*, 1010–1020.
[51] Tian, J. Q.; Liu, Q.; Asiri, A. M.; Sun, X. P. Self-supported nanoporous cobalt phosphide nanowire arrays: An efficient 3D hydrogen-evolving cathode over the wide range of pH 0–14. *J. Am. Chem. Soc.* **2014**, *136*, 7587–7590.
[52] Yang, H. C.; Zhang, Y. J.; Hu, F.; Wang, Q. B. Urchin-like CoP nanocrystals as hydrogen evolution reaction and oxygen reduction reaction dual-electrocatalyst with superior stability. *Nano Lett.* **2015**, *15*, 7616–7620.
[53] Pan, Y.; Lin, Y.; Chen, Y. J.; Liu, Y. Q.; Liu, C. G. Cobalt phosphide-based electrocatalysts: Synthesis and phase catalytic activity comparison for hydrogen evolution. *J. Mater. Chem. A* **2016**, *4*, 4745–4754.
[54] Tang, C.; Zhang, R.; Lu, W. B.; He, L. B.; Jiang, X.; Asiri, A. M.; Sun, X. P. Fe-Doped CoP nanoarray: A monolithic multifunctional catalyst for highly efficient hydrogen generation. *Adv. Mater.* **2017**, *29*, 1602441.
[55] Ji, Y. Y.; Yang, L.; Ren, X.; Cui, G. W.; Xiong, X. L.; Sun, X. P. Nanoporous CoP_3 nanowire array: Acid etching preparation and application as a highly active electrocatalyst for the hydrogen evolution reaction in alkaline solution. *ACS Sustainable Chem. Eng.* **2018**, *6*, 11186–11189.
[56] Liu, T. T.; Xie, L. S.; Yang, J. H.; Kong, R. M.; Du, G.; Asiri, A. M.; Sun, X. P.; Chen, L. Self-standing CoP nanosheets array: A three-dimensional bifunctional catalyst electrode for overall water splitting in both neutral and alkaline media. *ChemElectroChem* **2017**, *4*, 1840–1845.
[57] Gu, W. L.; Gan, L. F.; Zhang, X. Y.; Wang, E. K.; Wang, J. Theoretical designing and experimental fabricating unique quadruple multimetallic phosphides with remarkable hydrogen evolution performance. *Nano Energy* **2017**, *34*, 421–427.
[58] Liang, H. F.; Gandi, A. N.; Anjum, D. H.; Wang, X. B.; Schwingenschlögl, U.; Alshareef, H. N. Plasma-assisted synthesis of NiCoP for efficient overall water splitting. *Nano Lett.* **2016**, *16*, 7718–7725.
[59] Liu, S. D.; Sankar, K. V.; Kundu, A.; Ma, M.; Kwon, J. Y.; Jun, S. C. Honeycomb-like interconnected network of nickel phosphide hetero-nanoparticles with superior electrochemical performance for supercapacitors. *ACS Appl. Mater. Interfaces* **2017**, *9*, 21829–21838.
[60] Feng, Y.; Yu, X. Y.; Paik, U. Nickel cobalt phosphides quasi-hollow nanocubes as an efficient electrocatalyst for hydrogen evolution in alkaline solution. *Chem. Commun.* **2016**, *52*, 1633–1636.
[61] Xin, H.; Guo, K.; Li, D.; Yang, H. Q.; Hu, C. W. Production of high-grade diesel from palmitic acid over activated carbon-supported nickel phosphide catalysts. *Appl. Catal. B: Environ.* **2016**, *187*, 375–385.
[62] Yang, F. L.; Chen, Y. T.; Cheng, G. Z.; Chen, S. L.; Luo, W. Ultrathin nitrogen-doped carbon coated with CoP for efficient hydrogen evolution. *ACS Catal.* **2017**, *7*, 3824–3831.
[63] Zhang, F. S.; Wang, J. W.; Luo, J.; Liu, R. R.; Zhang, Z. M.; He, C. T.; Lu, T. B. Extraction of nickel from NiFe-LDH into Ni_2P@NiFe hydroxide as a bifunctional electrocatalyst for efficient overall water splitting. *Chem. Sci.* **2018**, *9*, 1375–1384.
[64] Conway, B. E.; Tilak, B. V. Interfacial processes involving electrocatalytic evolution and oxidation of H_2, and the role of chemisorbed H. *Electrochim. Acta* **2002**, *47*, 3571–3594.